

# Unoriented Adsorption of Interacting Spheroidal Particles

Zbigniew Adamczyk<sup>1</sup> and Paweł Weroński

*Institute of Catalysis and Surface Chemistry, Polish Academy of Sciences, ul.Niezapominajek 1, 30-239 Cracow, Poland*

Received November 25, 1996; accepted February 17, 1997

**Kinetics of localized adsorption of interacting spheroidal particles on homogeneous interfaces was analyzed theoretically. In contrast to previous studies, in our present approach an unoriented (quasi-3D) adsorption of prolate and oblate spheroids was considered. By applying the random sequential adsorption (RSA) method, numerical Monte Carlo type simulations were performed for colloidal particles interacting via a repulsive potential stemming from the electrostatic double-layers (exponentially decaying Yukawa-type potential). The surface blocking parameter (available surface function) and adsorption kinetics were determined for various particle shapes and for a broad range of the  $\kappa a$  parameter characterizing the range of the interaction potential. It was demonstrated that the "exact" numerical results can well be described for not too high surface concentrations by the approximate analytical expressions derived using the equivalent hard particle concept. On the other hand, for surface concentrations close to jamming, adsorption kinetics of interacting particles can well be approximated by the power-law dependencies analogous to hard particles. The theoretical analysis revealed that adsorption rate of colloid particles having a spheroidal shape is considerably diminished by the lateral electrostatic interactions.** © 1997 Academic Press

**Key Words:** adsorption; spheroidal particles; electrostatic interaction; particle adsorption kinetics; spheroidal particle adsorption.

## INTRODUCTION

Adsorption of colloid and bioparticles at solid/liquid interfaces is of large practical significance in various technologies involving filtration steps. Learning about mechanisms and kinetics of these phenomena is also relevant for polymer and colloid science, biophysics, and medicine enabling better control of protein and cell separation processes, enzyme immobilization, and prevention of thrombosis, biofouling of artificial organs, etc.

It should be noted that the shape of most surfactant molecules and bioparticles deviates from a spherical shape analyzed usually in various theoretical and experimental studies of adsorption kinetics. Various bacteria strains resemble elongated spheroids, e.g., the *E. Coli* bacteria having the width to length ratio of about 0.5 (1) or the bacteria from the *Actinomyces* group characterized by a much larger elongation (2).

Similarly, the shape of important globular proteins like bovine serum albumin (BSA) or fibrinogen (3–6) resembles prolate spheroids with the axis ratio about 0.28 and 0.2–0.18, respectively.

Other examples of highly anisotropic particles are the red blood cells, blood platelets, pigments, and synthetic inorganic colloids: gold, silver iodide, silver bromide, barium sulfate, etc. (7–9). Also, model polymeric colloid system of nonspherical monodisperse particles, e.g., PTFE or polystyrene latexes (10) or silica covered bohemite (11), can now be prepared in a reproducible way.

Adsorption of bioparticles and colloids proceeds usually via a more complex path than molecular adsorption and often appears irreversible due to specific interactions with the interfaces. Moreover, the kinetics of particle adsorption and structure of adsorbed layers can be influenced by external force fields (e.g., gravity or inertia in a centrifuge, magnetic forces) or hydrodynamic flows.

For higher surface concentrations the particles which accumulated at the interface disturb the local velocity and electrostatic fields and exert additional forces on adsorbing particle thereby excluding them from certain places at the interface. This leads to the surface-blocking effects (called also volume-excluding effects) which decrease particle adsorption rate for higher surface concentrations. An exact theoretical analysis of these effects seems rather cumbersome without accepting drastic simplifications concerning the many-body hydrodynamics and specific interactions among adsorbed and adsorbing particles (12–14).

One of the most widespread ways of accounting for the nonlinear effects is to introduce the surface blocking parameter  $B(\theta)$  (often referred to as the available surface function  $\phi$ ) as a natural extension of the Langmuir approach derived for gas adsorption (15).

For liquid phase adsorption, however, the Langmuir model does not seem to be appropriate, although, it may be useful for low surface concentrations (14). Nevertheless, due to its simplicity, the Langmuir model is widely used for describing the blocking effects of proteins (16–18), colloids (14, 19–23), and bacteria (24–25).

A more realistic theoretical determination of  $B$  for colloidal particles can be achieved using the recent theoretical

<sup>1</sup> To whom correspondence should be addressed.

models, especially various mutations of the random sequential adsorption (RSA) approach developed in (26–29).

Despite the simplicity of the underlying assumptions the topology of particle distributions generated in RSA processes becomes complex for higher surface concentrations and analytical solutions become possible only for one-dimensional (1D) adsorption (30–31). A proper description of the RSA process for spherical particles in 2D was achieved in terms of the Monte Carlo type computer simulations (14, 26–29, 32–33).

On the other hand, the RSA results for nonspherical particles are rather scarce and concern mostly noninteracting (hard) particles adsorbing flat (side on) such as cubes (34–35), cylinders (36), spherocylinders (37), and spheroids (37–38). In these cases adsorption can be treated as a two-dimensional (2D) process.

The side-on adsorption of prolate spheroids interacting via the screened electrostatic potential was recently studied in (39).

Despite its practical significance, however, no results were reported yet for interacting anisotropic particles which can undergo adsorption under an arbitrary orientation of the symmetry axis relative to the interface. This adsorption regime, referred to for sake of convenience as three-dimensional (3D) or unoriented adsorption, seems pertinent to surfactant and protein adsorption, especially at higher coverages when the flat orientation of molecules (or particles) is prohibited due to steric constraints.

Therefore, the goal of this paper is a quantitative description of the 3D adsorption kinetics of interacting spheroidal particles both of elongated (prolate spheroid) and flattened (oblate spheroid) shape. The theoretical model used in our work is based on the generalization of the RSA approach which enables one to perform not only the Monte Carlo type numerical simulations of adsorption processes but also to derive analytical expressions valid for low and moderate surface concentrations. Some preliminary results obtained for noninteracting (hard) particles have been presented in (40).

## THEORETICAL

### 1. General Considerations

We will describe the 3D adsorption of spheroidal particles in terms of the random sequential adsorption (RSA) model whose basic assumptions are:

(i) particle adsorption occurs at a microscopically homogeneous interface  $\Delta S$ ; i.e., the probability density  $dp$  of choosing a given particle position over the interface is uniform and the integral of  $dp$  over  $\Delta S$  is normalized to unity;

(ii) the probability density of particle adsorption in the vicinity of preadsorbed particles is governed by the Boltzmann distribution;

(iii) after adsorption particle positions and orientations

remain time independent; i.e., adsorption is postulated localized and irreversible.

Let the RSA process proceed for some time  $t$ . Then, there are  $N$  particles adsorbed at the interface whose positions are characterized by surface position vectors  $\mathbf{r}_1, \mathbf{r}_2, \dots, \mathbf{r}_N$  (which are projections of the corresponding 3D center position vectors on the adsorption plane) and the orientation vectors (of the symmetry axes)  $\hat{\mathbf{e}}_1, \hat{\mathbf{e}}_2, \dots, \hat{\mathbf{e}}_N$  (see Fig. 1). The position of the  $N + 1$  adsorbing (virtual) particle is characterized by the surface position vector  $\mathbf{r}_v$  and orientation vector  $\hat{\mathbf{e}}_v$  (Fig. 1).

According to assumption (ii), for this particle configuration, the probability density of placing the virtual particle within the infinitesimal surface element  $dS$  (located at the point  $\mathbf{r}_v$ ) under the orientation  $\hat{\mathbf{e}}_v$  is given by the Boltzmann law, i.e.,

$$dp(\mathbf{r}_1, \mathbf{r}_2, \dots, \mathbf{r}_N, \mathbf{r}_v, \hat{\mathbf{e}}_1, \hat{\mathbf{e}}_2, \dots, \hat{\mathbf{e}}_N, \hat{\mathbf{e}}_v) = e^{-\phi_v/kT} dS, \quad [1]$$

where  $k$  is the Boltzmann constant,  $T$  the absolute temperature, and  $\phi_v(\mathbf{r}_1, \mathbf{r}_2, \dots, \mathbf{r}_N, \mathbf{r}_v, \hat{\mathbf{e}}_1, \hat{\mathbf{e}}_2, \dots, \hat{\mathbf{e}}_N, \hat{\mathbf{e}}_v) > 0$  is the interaction energy of the adsorbing particle with all the previously adsorbed particles;  $\phi_v$  becomes infinite when particles overlap.

According to definition (14) the surface blocking parameter  $B$  is equal the probability of placing the virtual particle under a given orientation at the interface covered with particles, i.e.,

$$B(\hat{\mathbf{e}}_v) = p/p_0 = \int_{\Delta S} e^{-\phi_v/kT} d\mathbf{r}_v = 1 + \int_{\Delta S} f_v d\mathbf{r}_v, \quad [2]$$

where  $p_0 = 1$  according to assumption (i) and  $f_v = e^{-\phi_v/kT} - 1$  is the Mayer function of the virtual particle.

Obviously, the surface blocking parameter as defined above depends on positions and orientations of all adsorbed particles and the virtual particle. In order to determine an averaged value of  $B$  and eliminate the influence of the boundary conditions at the perimeter of the simulation plane one should consider large particle populations or take ensemble averages from many smaller surface elements.

An explicit analytical calculation of  $B$  by evaluating the double integral defined by Eq. [2] is not feasible, however, because the statistical properties of the irreversible RSA sequences cannot be deduced *a priori* and the interaction energy  $\phi_v$  for many-body systems is difficult to evaluate. Exact calculations of  $B$  can only be performed numerically using the Monte Carlo (MC) simulation techniques as discussed later.

However, useful analytical approximations can be derived for not-too-high surface concentration and short-ranged interaction potentials using the density expansion method (29, 33). According to this approach the surface blocking parameter can be expressed in terms of a polynomial of  $N$

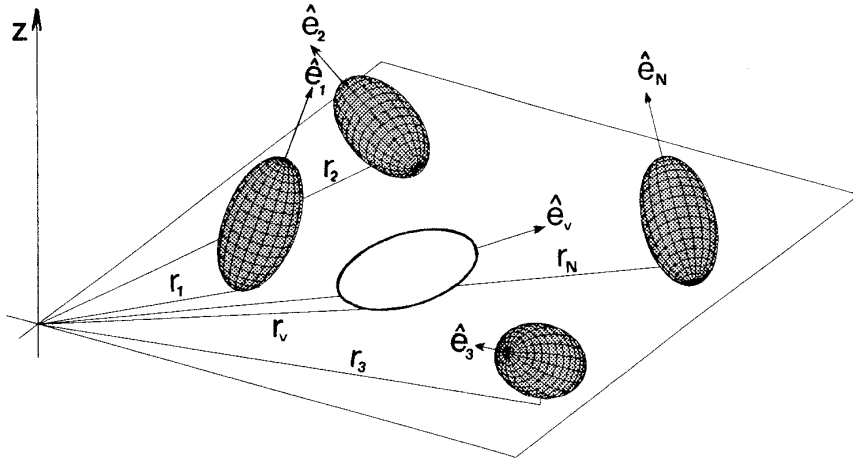


FIG. 1. A schematic representation of quasi-3D random sequential adsorption of spheroidal particles at a planar homogeneous interface.

$$B(\hat{\mathbf{e}}_v, N) = 1 - I_1(\hat{\mathbf{e}}_v)N + \frac{1}{2} I_2(\hat{\mathbf{e}}_v)N^2 - \dots, \quad [3]$$

where the multiple integrals  $I_1, I_2$  are given by

$$I_1(\hat{\mathbf{e}}_v) = - \iint g_0^{(1)}(\hat{\mathbf{e}}_v) f_{1v}(\mathbf{r}_v, \hat{\mathbf{e}}_1, \hat{\mathbf{e}}_v) d\mathbf{r}_v (d\hat{\mathbf{e}}_1/2\pi) \quad [4]$$

$$I_2(\hat{\mathbf{e}}_v) = \iiint g_0^{(2)}(\mathbf{r}_{12}, \hat{\mathbf{e}}_1, \hat{\mathbf{e}}_2, \hat{\mathbf{e}}_v) \times \left\{ \int [2I_1 + f_{2v}(\mathbf{r}_v, \mathbf{r}_{12}, \hat{\mathbf{e}}_1, \hat{\mathbf{e}}_2, \hat{\mathbf{e}}_v)] d\mathbf{r}_v \right\} \times d\mathbf{r}_{12} (d\hat{\mathbf{e}}_1/2\pi) (d\hat{\mathbf{e}}_2/2\pi), \quad [5]$$

where  $g_0^{(1)}$  and  $g_0^{(2)}$  are the one- and two-particle distribution functions (40),  $f_{1v} = e^{-\phi_{1v}/kT} - 1$ ,  $f_{2v} = e^{-\phi_{2v}/kT} - 1$ ,  $\phi_{1v}$  is the interaction energy of the virtual particle with a single adsorbed particle and  $\phi_{2v}$  is the interaction energy with a pair of adsorbed particles.

It should be noted that since  $\Delta S$  was normalized to unity, the  $N$  value in Eq. [3] can be treated as the surface concentration of adsorbed particles.

The series expansion Eq. [3] was truncated on the third term because

(i) the multiple integrals to be evaluated become vastly involved for the fourth and higher terms and

(ii) simple analytical expression for the kinetic equation describing the  $\theta$  vs time dependence can be derived.

Knowing the surface blocking parameter  $B$  for a given orientation of the virtual particle, one can describe the kinetics of spheroidal particle adsorption by the integral equation (35, 40)

$$\frac{dN}{dt} = \int k_a(\hat{\mathbf{e}}_v) g^{(1)}(\hat{\mathbf{e}}_v) B(\hat{\mathbf{e}}_v, N) (d\hat{\mathbf{e}}_v/2\pi), \quad [6]$$

where  $k_a(\hat{\mathbf{e}}_v)$  is the adsorption rate constant which can be interpreted as the reduced initial flux  $j_0/n_b$ ,  $n_b$  is the bulk concentration of particles (14), and  $g^{(1)}$  is the one-particle orientational distribution function.

It is interesting to mention that the initial flux for spheroidal particles has not been determined theoretically yet. However, for colloid particles and proteins characterized by  $a \ll 1 \mu\text{m}$  the interception and external force effects can be neglected and the diffusion boundary layer becomes much larger than particle dimensions (14). Then, the initial flux for spheroids can be estimated from the known results for spheres by introducing an equivalent diffusion coefficient.

An explicit formulation of Eq. [6] in the general case seems rather cumbersome. However, for many practical situations one can assume that  $k_a$  and  $g^{(1)}$  are independent of the orientation vector  $\hat{\mathbf{e}}_v$  (as is the case in the absence of external force fields orienting particles). Then, Eq. [6] can be simplified to the form

$$\frac{dN}{dt} = k_a n_b \bar{B}(N), \quad [7]$$

where  $\bar{B}(N) = \int B(\hat{\mathbf{e}}_v, N) (d\hat{\mathbf{e}}_v/2\pi)$  is the orientation-averaged surface blocking parameter.

Equations [3] and [7] can also be expressed in a more concise dimensionless form

$$\frac{d\theta}{d\tau} = B(\theta) = 1 - C_1\theta + C_2\theta^2 + 0(\theta^3), \quad [8]$$

where  $\theta = S_g N$  is the dimensionless concentration of adsorbed particles,  $S_g$  is the characteristic cross-section of the spheroid and  $\tau = k_a n_b S_g t$  is the dimensionless adsorption time.

The dimensionless constants  $C_1$  and  $C_2$  independent of  $\theta$  and the orientation angles are given by the expressions

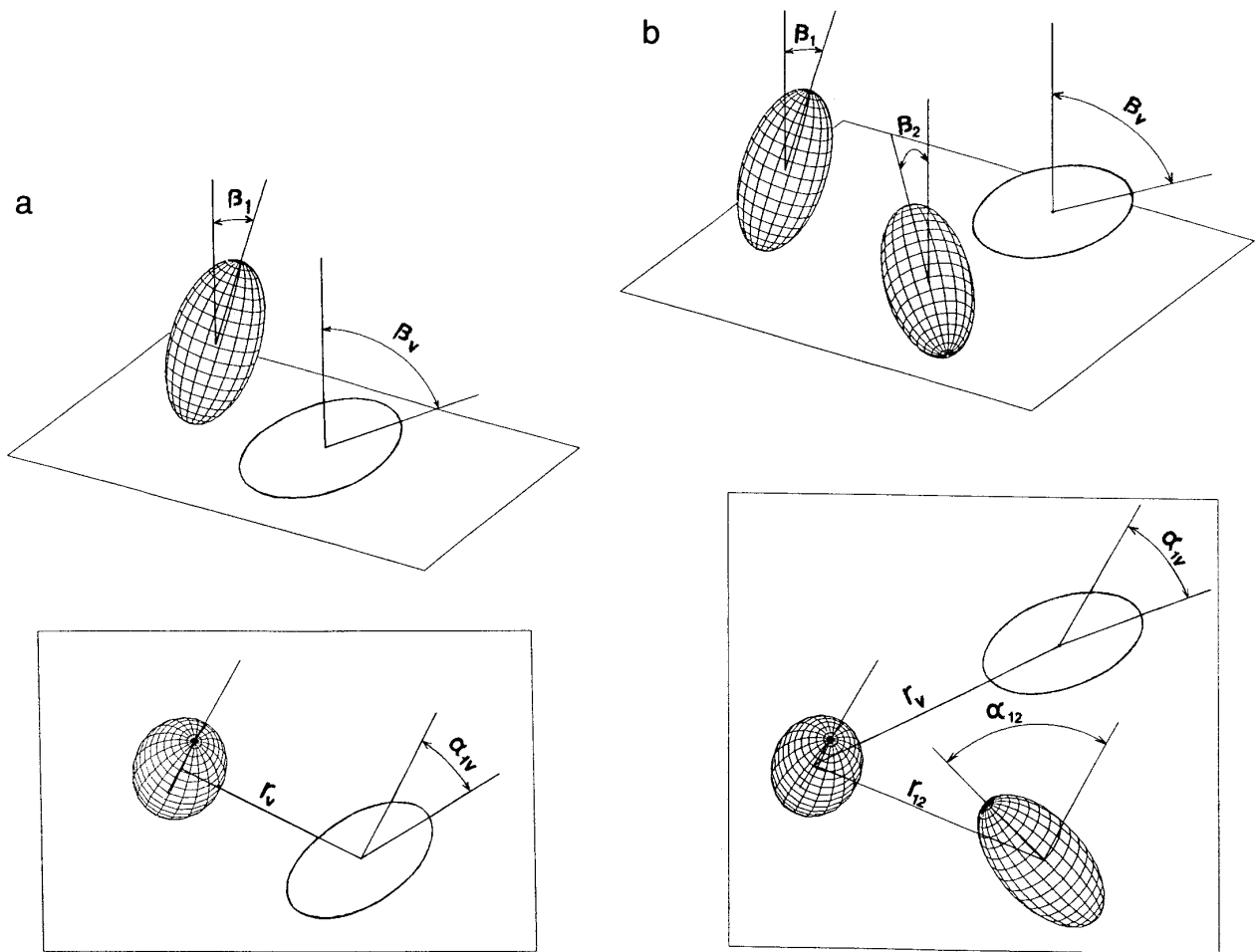


**FIG. 2.** (a) A perspective view (upper part) and the projection (lower part) of the two particle configuration occurring in calculations of the  $C_1$  constant (the adsorbed particle was shadowed). (b) The same as for (a) but for the three particle configuration occurring in calculations of the  $C_2$  constant.

$$C_1 = -\frac{2}{S_g \pi^3} \int_0^{2\pi} d\alpha_{1v} \int_0^{\pi/2} d\beta_1 \int_0^{\pi/2} d\beta_v \int f_{1v} d\mathbf{r}_v$$

$$C_2 = \frac{1}{S_g^2 \pi^5} \int_0^{2\pi} g_0^{(2)} d\alpha_{12} \int_0^{2\pi} d\alpha_{1v} \int_0^{\pi/2} d\beta_1 \int_0^{\pi/2} d\beta_2$$

$$\times \int_0^{\pi/2} d\beta_v \int d\mathbf{r}_{12} \int [2I_1 + f_{2v}] d\mathbf{r}_v, \quad [9]$$

where

$$f_1 = e^{-\bar{\phi}_1(\alpha_{1v}, \beta_1, \beta_v, \mathbf{r}_v)} - 1$$

$$f = e^{-\bar{\phi}_2(\alpha_{12}, \alpha_{1v}, \beta_1, \beta_2, \beta_v, \mathbf{r}_{12}, \mathbf{r}_v)} - 1$$

$\bar{\phi}_1 = \phi_1/kT$  is the dimensionless interaction energy of the virtual particle with a single adsorbed particle,  $\bar{\phi}_2 = \phi_2/kT$  is the dimensionless interaction energy of the virtual particle with a pair of adsorbed particles and  $g_0^{(2)} = e^{-\bar{\phi}_{1v}}$  is the zero-order pair correlation function (Boltzmann distribution). The angles  $\alpha_{12}$ ,  $\alpha_{1v}$ ,  $\beta_1$ ,  $\beta_2$ ,  $\beta_v$  derived from the orientation vectors  $\hat{\mathbf{e}}_1$ ,  $\hat{\mathbf{e}}_2$ ,  $\hat{\mathbf{e}}_v$  are defined in Fig. 2. Note that

due to symmetry the number of independent orientational coordinates is reduced by one.

It is interesting to mention that Eq. [8] can be integrated analytically which results in the following expression for particle adsorption kinetics (valid when  $4C_2/C_1^2 < 1$ )

$$\theta(\tau) = \theta_1 \frac{1 - \exp(-pC_1\tau)}{1 - \frac{\theta_1}{\theta_2} \exp(-pC_1\tau)}, \quad [10]$$

where

$$\theta_1 = \frac{C_1}{2C_2} [1 - p]; \quad \theta_2 = \frac{C_1}{2C_2} [1 + p]$$

$$p = \left(1 - \frac{4C_2}{C_1^2}\right)^{1/2}.$$

When,  $4C_2/C_1^2 > 1$  the solution becomes

$$\theta(\tau) = \frac{2tg((1/2)C_1p\tau)}{C_1p[1 + (1/p)tg((1/2)C_1p\tau)]};$$

$$p = \left(\frac{4C_2}{C_1^2} - 1\right)^{1/2}. \quad [11]$$

However, evaluation of the multiple integrals occurring in Eq. [9] and calculation of the  $C_1/C_2$  constants needed for approximation of particle adsorption kinetics can only be achieved numerically. This requires additionally that the interaction energies  $\bar{\phi}_1$  and  $\bar{\phi}_2$  are known for arbitrary configuration of clusters composed of two and three particles. The approximate method of calculating the electrostatic interaction energies of spheroidal particles is discussed in the next section.

## 2. Calculating the Interaction Energy

Due to the lack of exact solutions the electrostatic interaction energy of spheroidal particles was approximated using the usual additivity principle with the pair interactions calculated according to the equivalent sphere approach (ESA) described in some detail elsewhere (39, 41). The essence of this method consist in replacing the interaction of arbitrarily shaped convex bodies by interactions of two dissimilar spheres having the equivalent radii  $R_1$  and  $R_2$ . These are assumed equal the mean radii of curvature of the two particle evaluated at points of minimum separation.

The advantage of the ESA consist in the fact that many known numerical and analytical results concerning sphere interactions (41) can directly be transferred to spheroidal particles. Thus, for example, the commonly used expression derived for two spheres by accepting the linear superposition approach (LSA) can be generalized for spheroidal particles to the form

$$\phi = \epsilon \frac{(kT)^2}{e^2} Y^2 \frac{2R_1R_2}{R_1 + R_2 + h_m} e^{\kappa h_m}$$

$$= \phi_0 \frac{2\bar{R}_1\bar{R}_2}{\bar{R}_1 + \bar{R}_2 + H_m} e^{-\kappa a H_m}, \quad [12]$$

where  $\epsilon$  is the dielectric constant,  $e$  is the elementary charge,  $Y$  is the dimensionless functions of  $\kappa a$  and the electrokinetic potential of the particle  $\zeta_p$  which for thin double-layers, i.e., when  $\kappa a \gg 1$  becomes simply  $4th(\zeta_p e/4kT)$ ,  $\kappa^{-1} = Le = (\epsilon kT/8\pi e^2 I)$  is the Debye screening length,  $I$  is the ionic strength,  $a$  is the characteristic dimension of the spheroid (longer semiaxis),  $\bar{R}_1 = R_1/a$ ,  $\bar{R}_2 = R_2/a$  are the dimensionless mean radii of curvature of the two spheroids near the point of minimum separation,  $H_m = h_m/a$  is the dimensionless minimum distance between particle surfaces.

As discussed in (41) the accuracy of Eq. [12] is usually

decreased for small distances between spheroids ( $H_m \ll 1$ ) and thick double-layers when  $\kappa a < 1$ . This is no serious limitation, however, because at smaller distances the interaction energy assumes very large positive values and the Boltzmann factor tends to zero independently of the exact value of the energy.

It should also be mentioned that both the minimum separation distance  $h_m$  and the principal radii of curvature  $R_1$  and  $R_2$  depend in a complicated manner on the orientation of the spheroid pair and can be determined numerically only using the involved iterative procedure described elsewhere (39).

## THE NUMERICAL METHODS

### 1. Calculations of the Multiple Integrals

The  $C_1$  and  $C_2$  constants which have large significance for estimating surface blocking effects for low and moderate coverages were calculated from the defining integrals Eq. [9] by using the Monte Carlo integration method (42) based on the relationship

$$\int_{\Delta V} f dV = \langle f \rangle \Delta V, \quad [13]$$

where  $\Delta V$  is the domain of integration (of arbitrary dimension) and

$$\langle f \rangle = \frac{1}{N_t} \sum f_n$$

is the averaged value of the function  $f$  within  $\Delta V$  determined from  $N_t$  evaluations of  $f$  for points chosen at random within the multidimensional domain  $\Delta V$ . Usually, for obtaining a four digit accuracy about  $10^8/10^{10}$  evaluations of the integral of Eq. [9] were needed. Obviously, every evaluation required the determination of the interaction energy for a particle pair (in the case of the  $C_1$  constant) and for a cluster composed of three particles (in the case of the  $C_3$  constant). As mentioned, the pairwise energy additivity principle was assumed with the pair energy calculated from Eq. [12].

### 2. The MC-RSA Simulation Algorithm

In the general case of arbitrary surface concentration of spheroidal particles the blocking parameter  $B(\theta)$  and adsorption kinetics were calculated according to the algorithm being a generalization of the one previously used for the 2D adsorption (32–33, 39).

The simulation scheme consisted from three main calculation modules repeated in a loop:

(i) The virtual (adsorbing) spheroidal particle of a particle was generated having the coordinates  $(x_v, y_v)$  and the orientation  $\alpha_v, \beta_v$  measured relative to a space-fixed coordinate system (the  $z_v$  coordinate was unequivocally defined

by  $\beta_v$ ). The size of the square simulation plane  $\Delta S$  was normalized to unity and the relative cross-section surface area of the virtual particle  $S_g$  with respect to  $\Delta S$  was usually  $2 \times 10^{-4}$ . The periodic boundary conditions were applied at the perimeter of the simulation plane.

(ii) Then, the overlapping test was performed by scanning the adsorbing particle vicinity and using the Veillard-Baron (43) function. If overlapping occurred then step (i) was repeated, otherwise the minimum surface to surface distances between the virtual and previously adsorbed particles were determined by the procedure described in (39). Knowing the distances the net interaction energy  $\bar{\phi}$  was calculated as a sum of pair interactions using Eq. [12].

(iii) Finally, the virtual particle was adsorbed with the probability  $p_B$  given by the Boltzmann relationship. This was done by generating additional random number  $p_r$  with uniform distribution within the interval 0/1. If  $p_r < p_B$  then adsorption took place, if not, the simulation loop was repeated.

Since the RSA simulations were very time consuming (especially at higher surface concentrations) optimization of the algorithm was a crucial factor. As previously (32–33, 39) we introduced a three-dimensional subsidiary grid for enhancing the scanning efficiency of the adsorbing particle environment and used the efficient iterative method for determining the minimum surface to surface separation distances.

The blocking parameter  $B$  was calculated using the method described by Schaaf and Talbot (27–28). According to their procedure the RSA process was continued until a desired surface concentration was attained. Then, a large number of trials  $N_t$  of placing a new particle was performed by keeping the surface concentration constant. The number of successful attempts (would be adsorption events) was found to be  $N_{succ}$ . Taking advantage of the general large number probability law the blocking parameter  $B(\theta)$  was calculated as the limit of the ratio  $N_{succ}/N_t$  for  $N_t \rightarrow \infty$ .

On the other hand, particle adsorption kinetics was simulated directly by monitoring the number of successful adsorption events as a function of the dimensionless time  $\tau$  defined as (14)

$$\tau = \frac{t}{t_{ch}} = \frac{N_{att}}{N_{ch}} = \frac{N_{att}}{(1/S_g)}, \quad [14]$$

where  $N_{att}$  is the overall number of attempts at placing particles (repetitions of the simulation loop) and  $N_{ch}$  is the characteristic number of particles.

## RESULTS OF CALCULATIONS AND DISCUSSION

### 1. Calculations of the $C_1$ , $C_2$ Constants

The results of the numerical calculations of the  $C_1$  constant for prolate and oblate spheroids characterized by the aspect

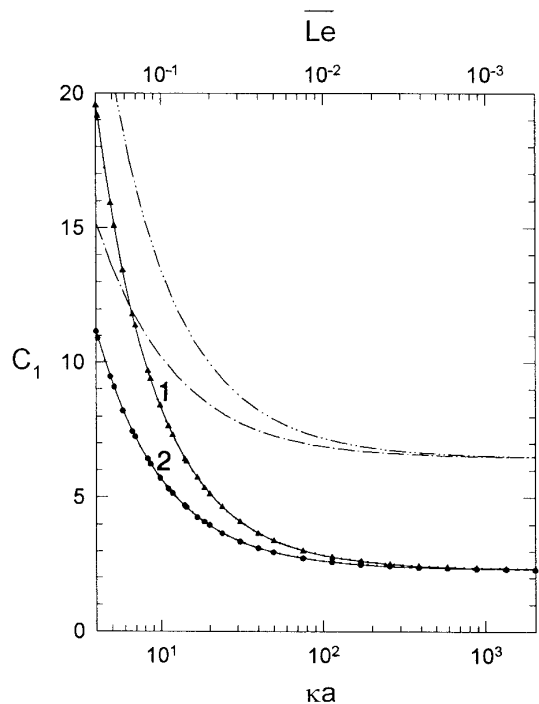


**FIG. 3.** The dependence of the  $C_1$  constant on the  $\kappa a$  ( $\bar{L}e$ ) parameter for interacting prolate spheroids ( $A = 0.2$ ). The filled triangles denote the numerical results calculated for the  $\phi_0$  parameter equal 1000 kT and the filled circles for  $\phi_0$  equal 100 kT. The solid lines denote the best fits calculated from Eq. [15]. The (-.-) lines represent the results obtained for the side-on (2D) adsorption.

ratio  $A = 0.2$  are shown in Figs. 3 and 4, respectively. We choose this value of  $A$  which is characteristic for some protein molecules often used in model adsorption studies, e.g., fibrinogen (4–6). Although in these adsorption studies the ionic strength value is rather high, i.e., 0.15  $M$  due to the small size of this protein (having the length  $2a$  about 450 Å) the  $\kappa a$  parameter assumed the value of about 28.

Therefore, in our calculations, whose results are shown in Fig. 3, we were primarily interested in determining theoretically the role of the  $\kappa a$  parameter in nonspherical particle adsorption.

The points in Fig. 3 represent the results of numerical evaluation of the integral Eq. [9] performed for a broad range of  $\kappa a$  and two values of  $\phi_0$ , i.e.,  $10^2$  and  $10^3$  kT, respectively. For comparison, the previously obtained results for the side-on adsorption are also plotted in Fig. 3. As can be seen, the dependence of  $C_1$  on  $\kappa a$  can well be described by the following interpolation polynomial of  $\kappa a^{-1} = \bar{L}e$  (cf. solid lines in Fig. 3)

$$C_1 = C_1^\infty + c_1 \bar{L}e + c_2 \bar{L}e^2, \quad [15]$$

where  $C_1^\infty = 2.314$  is the value of the  $C_1$  characteristic for noninteracting (hard) particles and  $c_1$ ,  $c_2$  dimensionless constants equal to 32.5 and 11.63 for  $\phi_0 = 100$  kT, and 53.62 and 62.67 for  $\phi_0 = 1000$  kT.

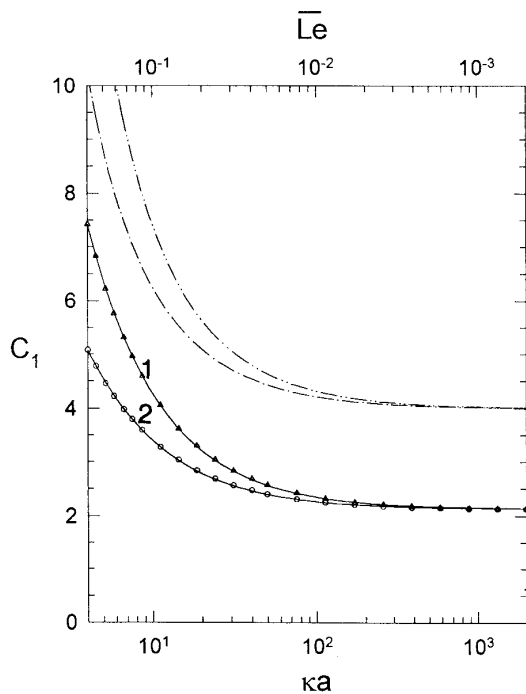


FIG. 4. The same as described in the legend for Fig. 3 but the oblate spheroids characterized by  $A = 0.2$ . The best fits were calculated from the Eq. [15]. The (-.-) lines denote the side-on (2D) adsorption (spheres).

The comparison between the side-on and the 3D (unoriented) adsorption suggest that in both cases the effect of the electrostatic interactions is very pronounced, especially for  $Le > 0.1$  ( $\kappa a < 10$ ) although the increase in  $C_1$  for  $Le > 0.1$  is steeper for the 3D adsorption. One can estimate that for the conditions characteristic for fibrinogen adsorption ( $\kappa a = 28$ ) the  $C_1$  constant becomes almost 50% larger than that for the hard particle case. Since  $C_1$  can be interpreted as the normalized surface area blocked by one molecule (in the limit of low surface coverages) one can deduce from the results shown in Fig. 3 that the blocking effects for interacting particles of elongated shape are considerably more pronounced than for the hard particles.

Similar results were obtained for oblate spheroids (cf. Fig. 4) which for  $A \ll 1$  resemble circular disks (40). In this case however, the increase in the blocking area for the side-on and 3D orientations seem to be very similar. It was found that also in this case the numerical results can well be interpolated by Eq. [15] with the coefficients

$$C_1^\infty = 2.134$$

$$c_1 = 13.24, c_2 = -6.10 \text{ for } \phi_0 = 100 \text{ kT and}$$

$$c_1 = 21.4, c_2 = -1.16 \text{ for } \phi_0 = 1000 \text{ kT.}$$

The calculations of the  $C_2$  constant according to the defining integral equation [9] were found to be considerably more time consuming. Therefore, we present results for prolate

spheroids only, characterized by  $A = 0.2$  (see Fig. 5). Analogously to the  $C_1$  constant, the value of  $C_2$  is considerably increased for lower  $\kappa a$  values. It is also interesting to observe that the numerical results shown in Fig. 5 can well be described, especially for  $\phi_0 = 100$  kT, by the geometrical scaling law formulated previously for the side-on adsorption (39), i.e.,

$$C_2 = 0.2965 C_1^2. \quad [16]$$

Equations [15]–[16] can be used for a convenient estimation of the  $C_1 - C_2$  constants for interacting prolate spheroids with a precision of a few percent. Additionally, by substituting these  $C_1 - C_2$  values into Eqs. [10]–[11] one can determine explicitly particle adsorption kinetics in the limit of low and moderate coverages with an accuracy sufficient for practical applications. However, the numerical evaluation of these constants seems rather tedious. Therefore, we present below the effective hard-particle concept which can be exploited for an efficient, analytical estimation of the  $C_1 - C_2$  constants and in consequence of the blocking parameter and adsorption kinetics for low and moderate surface concentrations.

## 2. The Effective Hard-Particle Approximation

The effective hard-particle concept was applied originally by Barker and Henderson (44) to describe the equation of

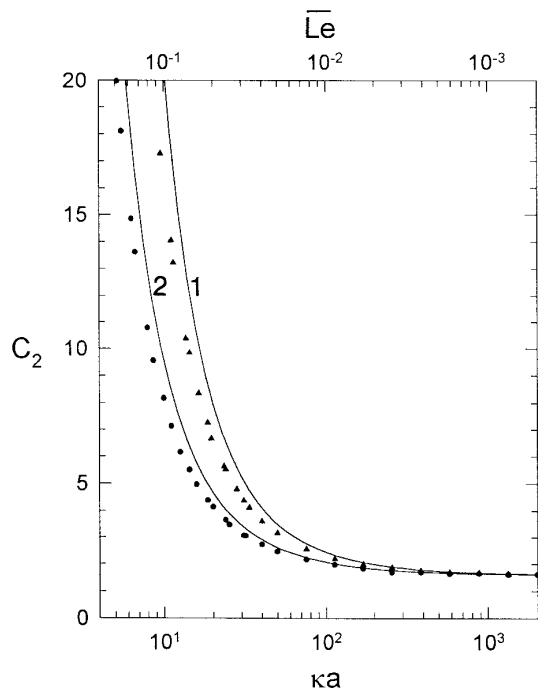


FIG. 5. The dependence of the  $C_2$  constant on the  $\kappa a$  parameter for interacting prolate spheroids ( $A = 0.2$ ); the filled triangles denote the numerical results calculated from Eq. [9] for  $\phi_0 = 1000$  kT and the filled circles for  $\phi_0 = 100$  kT. The solid lines denote the analytical results calculated from Eq. [16].

state of simple fluids of spherically shaped molecules. According to this approach, the interacting particles are treated as hard (noninteracting) ones having the equivalent dimension (radius)  $a^*$  increased over the geometrical dimension by  $h^*$ , i.e., the effective interaction range. Thus, the effective cross section of a spherical particle becomes simply  $S^* = \pi(a + h^*)^2$ . Consequently for spherical particles the  $C_1$  constant is connected with  $h^*$  by the parabolic dependence

$$C_1 = \frac{S^*}{S_g} = 4 \left( 1 + \frac{h^*}{a} \right)^2, \quad [17]$$

where  $S_g = \pi a^2$ .

This can easily be inverted giving for the dimensionless effective interaction range  $h^*/a$  the simple expression (39)

$$H^* = \frac{h^*}{a} = \frac{1}{2} \sqrt{C_1} - 1, \quad [18]$$

where the  $C_1$  constant is determined numerically by evaluating the integral Eq. [9] which for spherical particles simplifies to the form (14)

$$C_1 = 2 \int_0^\infty (1 - e^{-\bar{\phi}_1}) \bar{r} d\bar{r}. \quad [19]$$

$\bar{\phi}_1$  is the interaction energy of the pair of spheres and  $\bar{r}$  is the dimensionless distance between their centers.

In the side-on adsorption of spheroidal particles (ellipses), the dependence of  $C_1$  on  $H^*$  (analogous to Eq. [17]) becomes more involved. This is because the shape of the ‘‘parallel’’ figure obtained by increasing the size of an ellipse uniformly by the increment  $h^*$  deviates from the original elliptic shape and its surface area can only be expressed via the complete elliptic integral of the second kind (45–46). However, by applying an interpolation procedure analogous to that expressed by Eq. [15] one can show that  $C_1$  becomes also a parabolic function of  $H^*$

$$\begin{aligned} C_1 &= \frac{4(\pi^2 - 4)}{\pi^2} + \frac{8}{\pi^2} \left( A + \frac{1}{A} \right) \\ &+ 4 \left( 1 + \frac{1}{A} \right) H^* + \frac{4}{A} H^{*2} \\ &= C_1^\infty + c_1 H^* + c_2 H^{*2}. \end{aligned} \quad [20]$$

This can easily be inverted giving for  $H^*$  the expression

$$H^* = \frac{A+1}{2} \left[ \sqrt{1 + \frac{A}{(A+1)^2} (C_1 - C_1^\infty)} - 1 \right]. \quad [21]$$

The  $C_1$  constant can again be calculated by a numerical integration of Eq. [9] when substituting  $\beta_1 = \beta_2 = \beta_v = \pi/2$ .

In the case of unoriented adsorption of spheroidal particles, one can show by exploiting the hard-particle results presented in our previous work (39) that  $C_1$  for prolate spheroids assumes the form

$$C_1 = (2.07 + 0.811 A^* + 2.37 A^{*2} - 1.25 A^{*3}) \bar{S}_g^*, \quad [22]$$

where  $A^* = (A + H)/(1 + H)$  and  $\bar{S}_g^* = (1 + H^*)(1 + H^*/A)$ . Equation [22] can be transformed into the implicit fourth-order polynomial of  $H^*$  which can be inverted analytically (this involves the solution of a fourth-order algebraic equation) giving an explicit functional dependence of  $H^*$  on  $C_1$ . Since this expression was found to be very complicated, it is not reported here.

On the other hand, for oblate spheroids the interpolating expression for  $C_1$  becomes

$$C_1 = (1.59 + 2.80 A^* - 0.388 A^{*2}) \bar{S}_g, \quad [23]$$

where in this case  $\bar{S}_g^* = (1 + H^*)^2$ . Equation [23] can be evaluated and easily inverted (this involves a solution of a quadratic equation only) giving for  $H^*$  the expression fully analogous to Eq. [21], i.e.,

$$\begin{aligned} H^* &= \frac{5.98 + 2.02 A}{8} \\ &\times \left[ \sqrt{1 + \frac{16}{(5.98 + 2.02 A)^2} (C_1 - C_1^\infty)} - 1 \right], \end{aligned} \quad [24]$$

where  $C_1^\infty = 1.59 + 2.80 A - 0.388 A^2$  is the  $C_1$  constant for hard particles.

The results obtained for prolate spheroids using the equivalent hard-particle concept are plotted in Fig. 6 in the form of the dependence of  $H^*$  on the  $\kappa a$  ( $\bar{L}e$ ) parameter. As can be observed the numerical results (represented by points) obtained for various  $A$  values (and for  $\phi_0 = 1000$  kT) practically coincide for  $\kappa a > 10$  and moreover they seem to lie on a one straight line. This behavior confirms, therefore, the validity of the equivalent hard-particle concept, at least for this range of  $\kappa a$  values.

Very similar results were obtained for the oblate spheroids as well.

It should be mentioned that determination of the effective interaction range via the above-mentioned numerical method seems rather cumbersome for practical purposes. However, the character of the results shown in Fig. 6 suggests that they can be well-fitted by a linear dependence, i.e.,

$$H^* = \xi(\kappa a)^{-1} = \xi \bar{L}e. \quad [25]$$

The estimation of the proportionality constant can be achieved in analogy to previous results for the side-on ad-

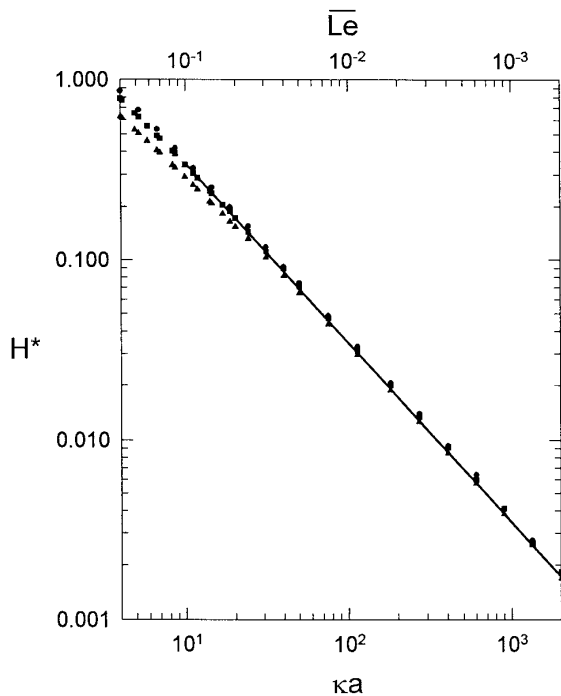


**FIG. 6.** The dependence of the effective interaction range  $H^*$  on the  $\kappa a$  ( $\bar{L}e$ ) parameter. The points represent exact numerical results for prolate spheroids derived for  $\phi_0 = 1000$  kT: (○)  $A = 1$  (spheres); (■)  $A = 0.5$ ; (△)  $A = 0.2$ ; the solid lines show the analytical approximation calculated from the equation  $H^* = \frac{1}{2} \bar{L}e \ln(\phi_0/\phi_{ch})$ .

sorption (39) using Eq. [12] and postulating that for  $H = H^*$  the pair interaction energy attains the characteristic value  $\phi_{ch}$ . In this way (by neglecting also the small variations of the preexponential term) one receives the simple expression

$$\xi = \frac{1}{2} \ln\left(\frac{\bar{\phi}_0}{\bar{\phi}_{ch}}\right). \quad [26]$$

Note that  $\xi$  is independent of the  $A$  parameter.

As can be seen in Fig. 6 the exact numerical results can indeed be described by the linear dependence Eq. [25] for a broad range of  $\bar{L}e$  values. The  $\phi_{ch}$  parameter was found close to a kT unity in accordance with physical expectations (being exactly 1.02 kT for prolate and 0.862 kT for oblate spheroids). This corresponds to  $\xi = 3.4$  and 3.5, respectively. As one can see from this estimation the effective interaction range for spheroidal particle adsorption proved to be significantly larger than the double layer thickness.

The results shown in Fig. 6 suggest, therefore, that the equivalent hard particle concept can be successfully used for approximating the blocking effects and consequently adsorption kinetics of interacting spheroidal particles. By using Eqs. [23]–[26] in combination with Eqs. [8], [10], and [11] one can express both  $B$  and  $\theta$  vs  $\tau$  for not-too-high surface concentrations in terms of the two experimentally accessible parameters the ionic strength of the suspension

and the zeta potential of the particle and the interface. However, the estimation of the range of validity of these approximate analytical expressions can only be achieved by comparison with exact numerical simulation of  $B(\theta)$  and the kinetic runs.

## RESULTS OF NUMERICAL SIMULATIONS

### 1. Calculations of $B(\theta)$

Using the above simulation scheme we calculated the dependence of the blocking parameter  $B$  on  $\theta$  both for prolate and oblate spheroids characterized by various values of the effective interaction range  $H^*$  defined above. Since the case of hard spheroids ( $H^* = 0$ ) has not been reported previously in the literature we have included them in our calculation scheme.

The results for hard prolate and oblate spheroids are shown in Figs. 7a and 7b, respectively. The calculations were performed for  $A = 0.5, 0.2$  and 0.1 (for comparison the case of spheres  $A = 1$  was also included). One can see in Figs. 7a and 7b that with decreasing  $A$  the blocking parameter  $B$  is increased. Also, the limiting “jamming” concentrations  $\theta_\infty$  (for which  $B = 0$ ) are considerably increased for smaller  $A$ . This is so because under the conditions of the 3D adsorption additional particles are adsorbing under orientations close to perpendicular so they need much smaller accessible surface area than for the side-on adsorption. This effect is especially well pronounced for  $A < 0.2$  both for prolate and oblate spheroids. As shown in (40) the jamming concentrations in the limit of  $A \rightarrow 0$  become inversely proportional to this parameter and can be described for prolate spheroids by the expression

$$\theta_\infty = 0.304 - 0.1234 A + \frac{0.365}{A}. \quad [27]$$

On the other hand, for oblate spheroids an analogous expression assumes the form

$$\theta_\infty = 0.768 - 0.473 A + \frac{0.251}{A}. \quad [28]$$

It should also be noted that the limiting low-coverage expansion Eq. [8] describes well the exact numerical calculations for a considerable range of  $\theta$  values, especially for the oblate spheroids.

The results obtained for interacting particles ( $A = 0.2, \phi_0 = 100$  kT) are shown for prolate spheroids in Fig. 8. As one can notice, similar to side-on adsorption (39), the increase in the  $H^*$  parameter (which according to Eq. [25] is proportional to  $\bar{L}e$ ) results in a significant decrease of  $B$  for the same surface coverage  $\theta$ ; i.e., the blocking effects become more pronounced when  $H^*$  increases.

It is also interesting to observe that the dependence of  $B$

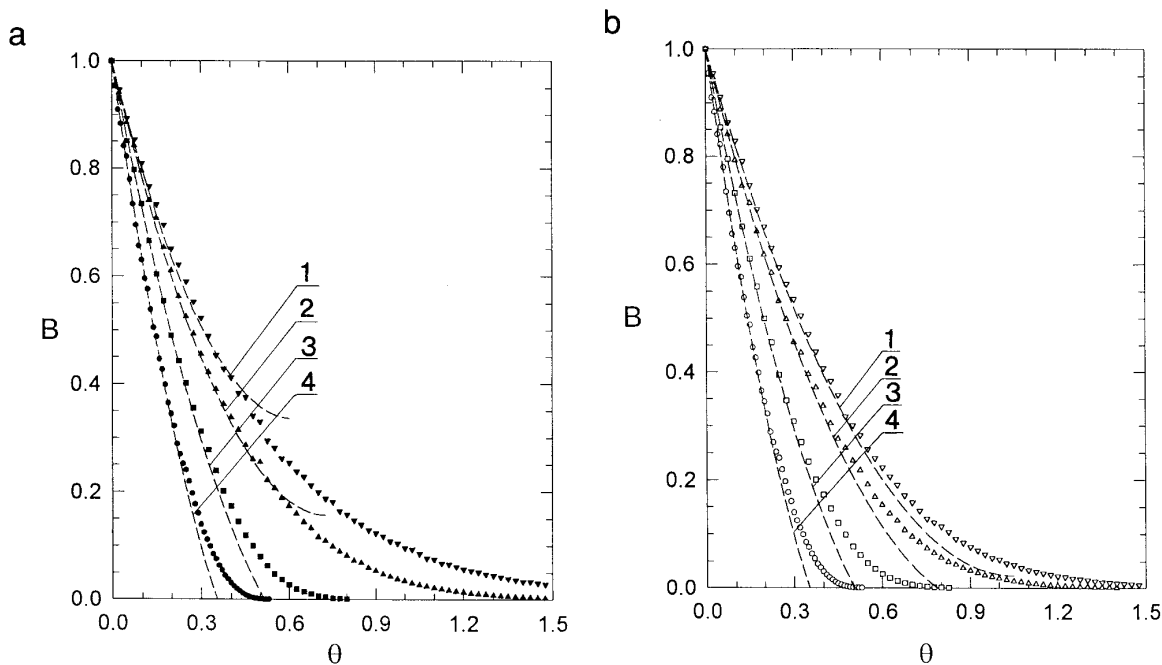


**FIG. 7.** (a) The dependence of the surface blocking parameter  $B$  (the ASF) on the dimensionless surface concentration  $\theta$  for hard prolate spheroids; the points denote the results of numerical simulations performed for: 1.  $A = 0.1$ ; 2.  $A = 0.2$ ; 3.  $A = 0.5$ ; 4.  $A = 1$  (spheres). The broken lines lines represent the low coverage analytical results calculated from Eq. [8]. (b) Same as for (a) but for oblate spheroids: 1.  $A = 0.1$ ; 2.  $A = 0.2$ ; 3.  $A = 0.5$ ; 4.  $A = 1$  (spheres). The broken lines lines represent the low coverage analytical results calculated from Eq. [8].

on  $\theta$  for interacting spheroidal particles becomes for some limiting  $H^*$  value almost identical with the hard-sphere case. This occurs, for example, for prolate spheroids at  $H^* = 0.15$  and for oblate spheroids for  $H^* = 0.25$ . Thus, due

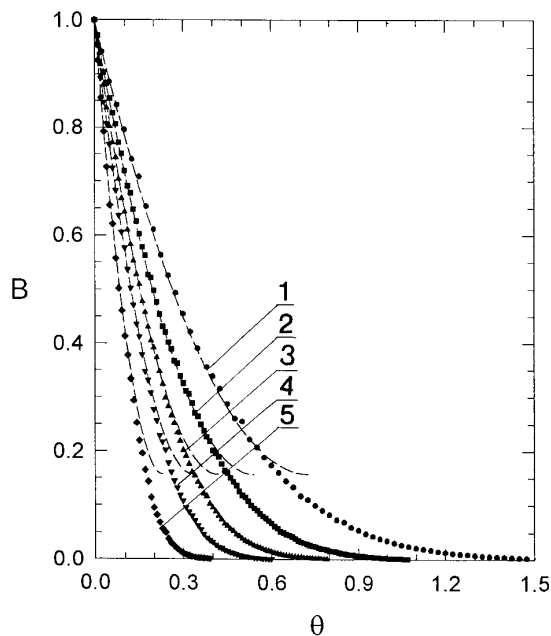


**FIG. 8.** The dependence of  $B$  on  $\theta$  for interacting prolate spheroids ( $A = 0.2$ ); the points denote the numerical simulations performed for: 1.  $H^* = 0$  (hard particles); 2.  $H^* = 0.05$ ; 3.  $H^* = 0.1$ ; 4.  $H^* = 0.15$ ; 5.  $H^* = 0.25$ . The continuous lines represent the analytical results calculated from Eq. [8].

to compensation of the two contradictory effects, i.e., the unoriented adsorption and electrostatic repulsion, adsorption processes of interacting spheroidal particles may apparently become very similar, (under a certain combination of the parameters  $A$ ,  $\kappa a$ , and  $\phi_0$ ) to adsorption of hard particles of spherical shape.

The natural coordinate system used in Figs. 7–8, i.e.,  $B(\theta)$  vs  $\theta$ , is useful for presenting the data for low surface concentrations only. For higher coverages the differences between the curves calculated for various  $A$  are difficult to observe. This should be more clearly visible when comparing the kinetic curves as discussed below.

## 2. Kinetics of Particle Adsorption

Some characteristic results (obtained using the above-described RSA simulation procedure) which illustrate the influence of the effective interaction range  $H^*$  on adsorption kinetics of prolate spheroids ( $A = 0.2$ ,  $\phi_0 = 100$  kT) are shown in Fig. 9a for the dimensionless adsorption time  $\tau < 5$ .

As can be observed in Fig. 9a the increase in the  $H^*$  parameter resulted in a considerable decrease in particle adsorption kinetics. This is why for  $H^* = 0.15$  the kinetic curve characteristic for elongated spheroids is very similar to the curve describing hard sphere adsorption.

It should also be noted that the limiting analytical solutions Eqs. [10]–[11] describe for  $\tau < 2$  reasonably well the exact numerical results, especially for smaller  $H^*$  values.

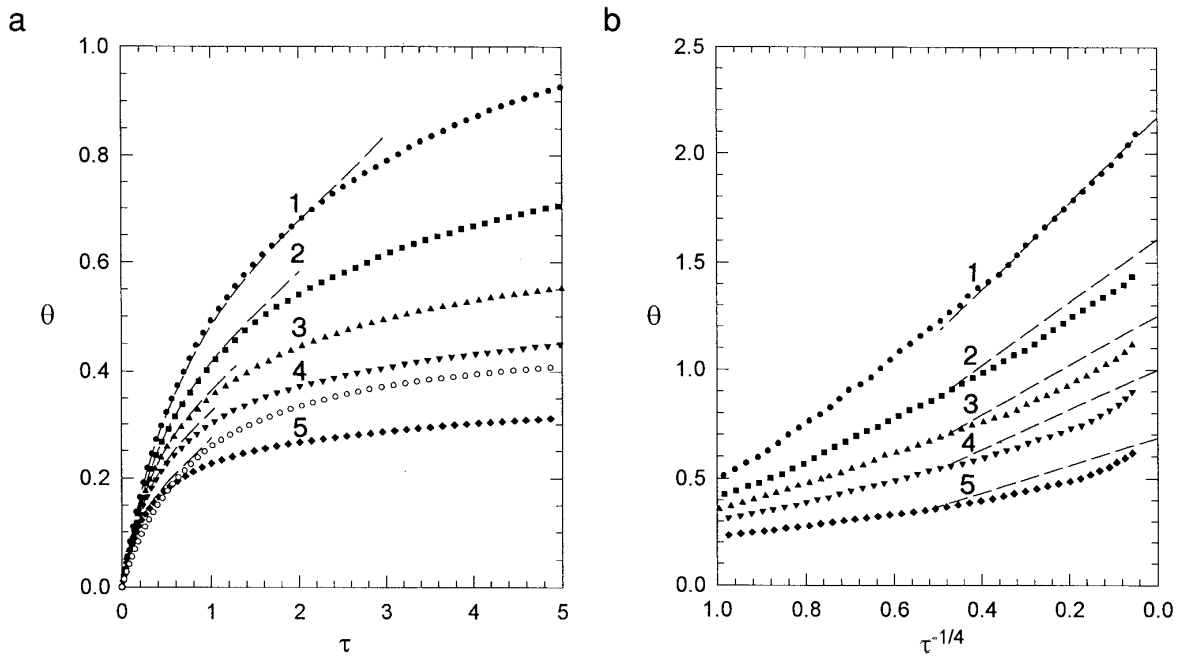


**FIG. 9.** Adsorption kinetics of interacting prolate spheroids (0.2). (a) The dependence of  $\theta$  on  $\tau$ . The points denote numerical simulations performed for: 1.  $H^* = 0$  (hard particles); 2.  $H^* = 0.05$ ; 3.  $H^* = 0.1$ ; 4.  $H^* = 0.15$ ; 5.  $H^* = 0.25$ . The broken lines represent the analytical approximation calculated from Eq. [11]. The empty symbols denote the results obtained for hard spherical particles. (b) The dependence of  $\theta$  on  $\tau^{-1/4}$  simulated numerically for: 1.  $H^* = 0$  (hard particles); 2.  $H^* = 0.05$ ; 3.  $H^* = 0.1$ ; 4.  $H^* = 0.15$ ; 5.  $H^* = 0.25$ . The broken lines show the analytical results calculated from Eq. [29].

However, due to the considerable decrease in particle adsorption rate for  $\tau > 2$  (which apparently may suggest that saturation values of  $\theta$  are approached) the kinetic curves cannot be effectively presented when using the natural coordinate system  $\theta$  vs  $\tau$ . The previous theoretical results concerning the asymptotic adsorption kinetics of hard spheroids in 3D indicate that the following transformation should be used to express adsorption kinetics for long times

$$\theta_{mx} - \theta = K\tau^{-1/4} \quad [29]$$

where  $K$  is the proportionality constant.

This suggests that the use of the  $\theta$  vs  $\tau^{-1/4}$  coordinate system should be more appropriate for  $\tau \gg 1$ . This transformation has an additional advantage of compressing the infinite  $\tau$  domain into a finite one. Such plots derived from numerical simulations performed for various  $H^*$  and  $A = 0.2$  prolate are shown in Fig. 9b. As can be observed, by using this transformation, the kinetic data can indeed be expressed as linear dependencies for a broad range of  $\tau$  for both hard and interacting particles.

Some small positive deviations from the linearity occurred at extremely long times ( $\tau^{-1/4} < 0.1$  which corresponds to  $\tau > 10^4$ ) in accordance with previous results for the side-on adsorption (39). This effect can in principle be accounted for by analyzing the target size and topology for the asymptotic regime close to jamming. We did not attempt to speculate further on this matter because the dimensionless adsorp-

tion times exceeding  $10^4$  are very difficult to attain in usual experiments involving proteins and colloids [14]. Moreover, for such extreme times the RSA assumptions are violated as mentioned later on.

Instead, we tried to fit the linear regimes by exploiting again the effective hard particle concept for calculating the jamming values  $\theta_{mx}$  of interacting spheroids from the relation used previously for the side-on adsorption (39)

$$\theta_{mx} = \theta_{\infty} \frac{{}^0C_1}{C_1(H^*)}. \quad [30]$$

Using Eq. [22] one can formulate Eq. [30] explicitly as

$$\theta_{mx} = \frac{(2.07 + 0.811 A + 2.37 A^2 - 1.25 A^3)}{(2.07 + 0.811 A^* + 2.37 A^{*2} - 1.25 A^{*3}) \times (1 + H^*)(1 + (H^*/A))} \quad [31]$$

with  $A^* = (A + H^*)/(1 + H^*)$ ,  $H^* = 1/2\kappa a \ln(\phi_0/\phi_{ch})$ . Then, substituting  $\theta_{mx}$  into Eq. [29] one obtains the linear fitting functions.

It can be seen in Fig. 9b that this approach gives rather satisfactory results for  $A = 0.2$  although a definite tendency to overestimate the numerical data is clearly visible. This is probably due to the orientation distribution anisotropy expected for surface concentrations close to the jamming. Since for this adsorption regime the spheroids can only ad-

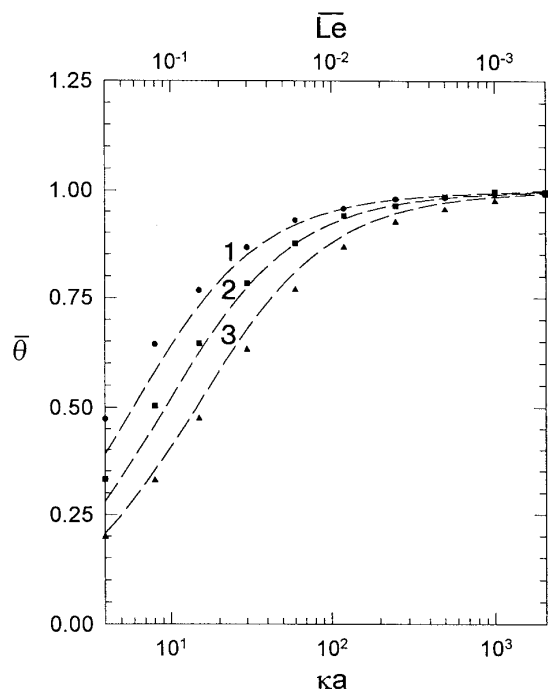


**FIG. 10.** The dependence of the normalized maximum surface concentration  $\theta_{mx}/\theta_\infty$  on the  $\kappa a$  parameter. The points denote the results of numerical simulation performed for interacting prolate spheroids ( $\phi_0 = 100$  kT): 1.  $A = 1$  (spheres); 2.  $A = 0.5$ ; 3.  $A = 0.2$ . The broken lines denote the analytical approximations calculated from Eq. [31].

sorb under an orientation close to perpendicular the interaction energy is increased. This results in turn in an decrease in adsorption kinetics below the value calculated from Eq. [27] formulated by assuming a uniform probability of particle orientations.

The maximum surface coverages stemming from Eq. [31] are plotted in Fig. 10 in the reduced form, i.e., as the dependence of  $\theta_{mx}/\theta_\infty$  on the  $\kappa a$  parameter. Using such a coordinate system is advantageous because the effect of the electrostatic interactions ( $\kappa a$  value) on the maximum surface coverages of spheroidal particles can clearly be visible. It should also be mentioned that the  $\theta_{mx}$  values are of a primary interest in protein adsorption studies (3–6, 16–18). As can be seen in Fig. 10 the approximate analytical estimations calculated from Eq. [31] are in good agreement with the exact numerical simulations for a broad range of  $\kappa a$  values, including the case characteristic for protein adsorption. Thus, the results shown in Fig. 10 seem useful since they indicate that the concept of the effective interaction range is valid for surface coverages close to jamming. This provides one with an efficient method of estimating via Eq. [31] the jamming coverages for interacting particles of nonspherical shape.

It is interesting to observe that by substituting Eq. [29] into Eq. [8] and differentiating one can derive for  $B(\theta)$  the relationship

$$B(\theta) = \frac{1}{4K^4} (\theta_{mx} - \theta)^5. \quad [32]$$

It should be mentioned that the RSA model discussed in our paper, although very useful due to its simplicity, has certain limitations which are expected to play a role for higher surface concentrations. They originate from neglecting the true 3D distribution of interaction energy between the virtual and preadsorbed particles and its translational and rotary Brownian motion. A proper consideration of these effects could only be possible by using the Brownian dynamics simulation method (14). At the present time, however, such simulations for systems of nonspherical particles seem prohibitive.

The success of the RSA approach in the case of spherical particles (14, 41) would suggest that also for nonspherical particles our theoretical results should prove useful for nonspherical particles as well. However, no direct quantitative verification of the hypothesis has been performed.

### CONCLUDING REMARKS

The theoretical analysis based on the RSA model showed that the surface-blocking parameter for interacting spheroidal particles in 3D can be approximated by the polynomial expression Eq. [8] valid for low and moderate surface concentrations  $\theta$ .

By adopting the effective hard-particle concept instead of evaluating these integrals numerically, one can formulate the analytical expressions for  $C_1$  in terms of  $H^*$  (cf Eqs. [22]–[26]). The effective interaction range  $H^*$  can be approximated by

$$H^* = (\kappa a)^{-1} \frac{1}{2} \ln \left( \frac{\bar{\Phi}_0}{\bar{\Phi}_{ch}} \right) = \bar{L}e \xi.$$

The dimensionless proportionality constant  $\xi$  is on the order 2–4 for particle sizes about 0.1  $\mu\text{m}$  and zeta potentials about 50 mV.

The exact numerical simulations performed according to the MC-RSA algorithm confirmed the validity of the above analytical expressions for predicting particle adsorption kinetics for  $\tau < 2$ .

It was also found that the effective hard particle concept can be used for higher surface concentrations as well with the blocking parameter expressed by the power law dependence Eq. [29] analogous to the hard particle case.

These analytical results and the extensive numerical simulations of adsorption kinetics suggest that the surface blocking effects become particularly pronounced for elongated particles when  $A < 0.5$ .

### REFERENCES

1. Xia, Z., Woo, L., and van de Ven, T. G. M., *Biorheology* **26**, 359 (1989).
2. Bos, R., van der Mei, H. C., Meinders, J. M., and Busscher, H. J., *J. Microbiol. Methods* **20**, 289 (1994).

3. Yoon, J. Y., Park, H. Y., Kim, J. H., and Kim, W. S., *J. Colloid Interface Sci.* **177**, 613 (1996).
4. Fowler, E., and Erickson, H. P., *J. Mol. Biol.* **134**, 241 (1979).
5. Schaaf, P., Dejardin, Ph., and Schmitt, A., *Langmuir* **3**, 1128, 1131 (1988).
6. Schaaf, P., and Dejardin, Ph., *Colloids Surf.* **31**, 89 (1988).
7. Sugimoto, T., *Adv. Colloid Interface Sci.* **28**, 65 (1987).
8. Peters, J. J., and Dezelic, G., *J. Colloid Interface Sci.* **50**, 296 (1975).
9. Ocana, M., Andres, M., Martinez, M., Serna, C. J., and Matijevic, E., *J. Colloid Interface Sci.* **163**, 262 (1994).
10. Ho, C. C., Keller, A., Odell, J. A., and Otewill, R. H., *Colloid Polym. Sci.* **271**, 469 (1993).
11. Wirenga, A. M., and Philipse, A. P., *J. Colloid Interface Sci.* **180**, 360 (1996).
12. van Megen, W., and Snook, I., *Faraday Discuss. Chem. Soc.* **76**, 151 (1983).
13. Ansell, G. S., and Dickinson, E., *Faraday Discuss. Chem. Soc.* **83**, 167 (1987).
14. Adamczyk, Z., Siwek, B., Zembala, M., and Belouschek, P., *Adv. Colloid Interface Sci.* **48**, 151 (1994).
15. Langmuir, I., *J. Am. Chem. Soc.* **10**, 1361 (1918).
16. Feder, J., and Giaever, I. J., *Colloid Interface Sci.* **78**, 144 (1980).
17. Young, B. R., Pitt, W. G., and Cooper, S. I., *J. Colloid Interface Sci.* **124**, 28 (1988).
18. Aptel, J. D., Voegel, J. C., and Schmitt, A., *Colloids Surf.* **29**, 359 (1988).
19. Vincent, B., Young, C. A., and Tadros, Th. F., *J. Chem. Soc. Faraday Trans. 1* **76**, 665 (1980).
20. Vincent, B., Jafelicci, and M., Luckham, P. F., *J. Chem. Soc. Faraday Trans. 1* **76**, 674 (1980).
21. Kallay, N., Tomic, M., Biskup, B., Kunjasic, I., and Matijevic, E., *Colloids Surf.* **28**, 185 (1985).
22. Dąbroś, T., and van de Ven, T. G. M., *Colloid Polymer Sci.* **261**, 694 (1983).
23. Dąbroś, T., and van de Ven, T. G. M., *J. Colloid Interface Sci.* **89**, 232 (1982).
24. Gibbons, R. J., Moreno, E. C., and Etherden, I., *Infect. Immun.* **39**, 280 (1983).
25. Moncla, B. J., Halfpap, L., and Birdsell, D. C., *J. Gen. Microbiol.* **131**, 2619 (1985).
26. Hinrichsen, E. L., Feder, J., and Jossang, T., *J. Stat. Phys.* **44**, 793 (1986).
27. Schaaf, P., and Talbot, J., *J. Chem. Phys.* **91**, 4401 (1989).
28. Schaaf, P., and Talbot, J., *Phys. Rev. Lett.* **62**, 175 (1989).
29. Evans, J. W., *Rev. Modern Phys.* **65**, 1281 (1993).
30. Widom, B., *J. Chem. Phys.* **44**, 3888 (1966).
31. Widom, B., *Chem. Phys.* **58**, 4043 (1973).
32. Adamczyk, Z., Zembala, M., Siwek, B., and Warszyński, P., *J. Colloid Interface Sci.* **140**, 123 (1990).
33. Adamczyk, Z., Siwek, B., and Zembala, M., *J. Colloid Interface Sci.* **151**, 351 (1992).
34. Finegold, L., and Donell, J. T., *Nature* **278**, 443 (1979).
35. Viot, P., and Tarjus, G., *Europhys. Lett.* **13**, 295 (1990).
36. Vigil, R. D., and Ziff, R. M., *J. Chem. Phys.* **91**, 2599 (1989).
37. Ricci, S. M., Talbot, J., Tarjus, G., and Viot, P., *J. Chem. Phys.* **97**, 5219 (1992).
38. Talbot, J., Tarjus, G., and Schaaf, P., *Phys. Rev. A* **40**, 4808 (1989).
39. Adamczyk, Z., and Weroński, P., *Langmuir* **11**, 4400 (1995).
40. Adamczyk, Z., and Weroński, P., *J. Chem. Phys.* **105**, 5562 (1996).
41. Adamczyk, Z., and Warszyński, P., *Adv. Colloid Interface Sci.* **63**, 41 (1996).
42. Press, W. H., Teukolsky, S. A., Vetterling, W. T., and Flannery, B. P., "Numerical Recipes in Fortran," second ed., p. 266. Cambridge Univ. Press 1992.
43. Vieillard-Baron, J., *J. Chem. Phys.* **56**, 4729 (1972).
44. Barker, J. A., and Henderson, D., *J. Chem. Phys.* **47**, 4714 (1967).
45. Boublik, T., *Mol. Phys.* **29**, 421 (1975).
46. Tarjus, G., Viot, P., Ricci, S. M., and Talbot, J., *Mol. Phys.* **4**, 773 (1991).